Solar MHD Theory and Observations: A High Spatial Resolution Perspective
ASP Conference Series, Vol. 354, 2006
Uitenbroek, Leibacher, and Stein

The Role of MHD Mode Conversion in Sunspot Seismology

A. D. Crouch[1,2,3], P. S. Cally[3], P. Charbonneau[2], D. C. Braun[4], and M. Desjardins[2]

[1]*Canadian Space Agency, 6767 Route de l'Aéroport, Longueuil, QC, J3Y 8Y9, Canada*
[2]*Département de Physique, Université de Montréal, QC, H3C 3J7, Canada*
[3]*Centre for Stellar and Planetary Astrophysics, School of Mathematical Sciences, Monash University, Victoria, 3800, Australia*
[4]*NorthWest Research Associates, Inc., Colorado Research Associates Division, 3380 Mitchell Lane, Boulder CO 80301-5410, USA*

Abstract. Sunspots absorb energy from and shift the phase of f and p modes incident upon them. Understanding the mechanism causing each of these effects is vital to the local helioseismology of sunspots (and magnetic flux concentrations in general). Because the beta-equals-unity layer typically lies in the near surface layers below the photospheres of sunspot umbrae, MHD mode conversion can occur. Mode conversion provides a promising absorption mechanism because the slow magnetoacoustic-gravity waves and Alfvén waves guide energy along the magnetic field away from the acoustic cavity. Our previous mode conversion calculations have shown that simple sunspot models with non-vertical magnetic fields can produce ample absorption to explain the Hankel analysis measurements, along with phase shift predictions that agree well with the observations. Those calculations only considered the possibility of MHD waves propagating down the magnetic field into the interior. In this contribution, we consider a second additional possibility – waves propagating up into the atmosphere overlying sunspots.

1. Introduction

Sunspots absorb energy from and shift the phase of f and p modes incident upon them (*e.g.*, Braun 1995). Recent modelling efforts by Crouch & Cally (2003, 2005), Cally et al. (2003), and Crouch et al. (2005) have demonstrated that both effects can be explained by simple sunspot models provided the magnetic field inclination is taken into account. In the first part of this contribution we summarise the essential findings of the most recent investigation (Crouch et al. 2005). In the last part we use a simple model for the upper atmosphere (based on isothermal slabs) to evaluate the influence of the top boundary condition and to test the validity of the boundary condition that was employed by Crouch et al. (2005).

2. The Model

The background model, for the variation of the gas pressure, density, adiabatic index, and local gravitational acceleration with depth, is based on the realistic solar model `fgong.l5bi.d.15` from the Aarhus adiabatic pulsation package (Christensen-Dalsgaard 1997). To this model we introduce a magnetic field that is straight and uniform, $\mathbf{B} = \mathrm{B}\,(\sin\theta\,\hat{\mathbf{e}}_x + \cos\theta\,\hat{\mathbf{e}}_z)$, where θ is the angle between the magnetic field and the vertical, $\hat{\mathbf{e}}_z$, and B is the field strength (curvature of the solar surface is neglected). The background model is modified to account for the effects of the magnetic pressure (the total pressure is independent of field strength). The variation of the sound speed for models of differing field strength is displayed in Figure 1. The influence of the magnetic pressure is strongest near the surface, which causes the sound speed to be reduced in models with larger field strength. On the other hand, at great depth, the gas pressure overwhelms the magnetic pressure and so there is little difference between the sound speed profile of the various models. Details of the variation in Alfvén speed and adiabatic exponent can be found in Crouch et al. (2005).

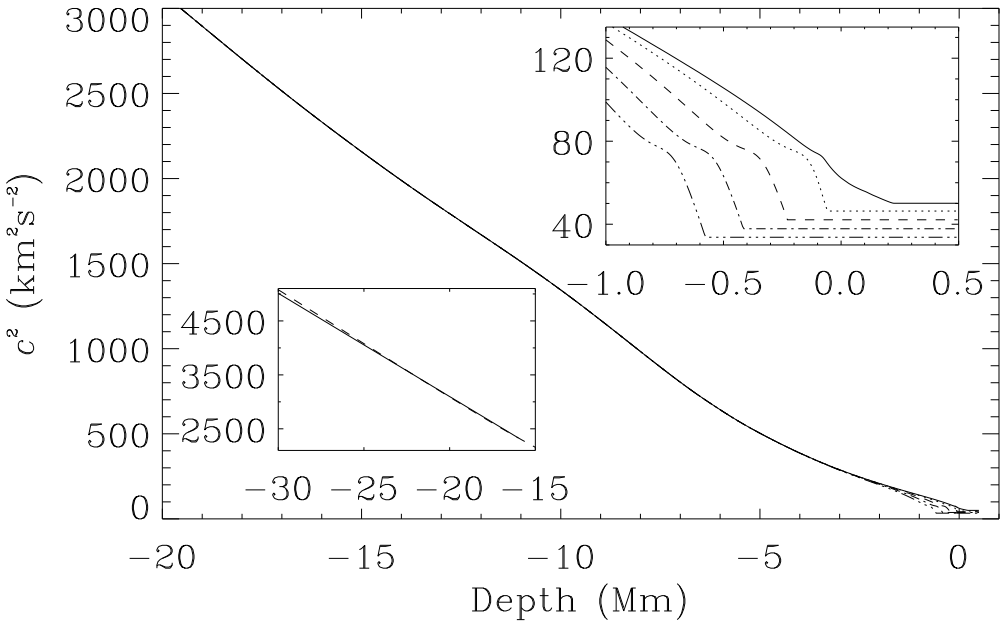

Figure 1. Squared sound speed, c^2, as a function of depth for the non-magnetic model and four of the magnetised models. The *full curve* is the squared sound speed for the non-magnetic model, the *dotted curve* is $B =$ 1 kG, the *dashed curve* is $B = 2$ kG, the *dash-dotted curve* is $B = 3$ kG, and the *dash-dot-dotted curve* is $B = 4$ kG. The *inset on the upper right* shows an expanded view of the surface layers. The *inset on the lower left* provides a comparison between the modified `fgong.l5bi.d.15` model with $B = 2$ kG (*dashed curve*) and the corresponding polytrope (*full curve*), that was used to develop asymptotic solutions for the wave equations at great depth.

The linearized MHD wave equations are then solved in each of the background models (which are assumed to be horizontally uniform for the moment). At this

stage, we will not concern ourselves with modelling wave propagation in the upper atmosphere (which is complicated by field non-uniformity and non-linear wave dynamics Rosenthal et al. 2002; Bogdan et al. 2003). Consequently, at the top of each model ($z = 500$ km), we impose rigid lid boundary conditions (each component of the displacement vector vanishes). At great depth in the model, asymptotic solutions for the wave equations can be developed, which allow us to impose physical boundary conditions: wave-like disturbances must be outgoing and evanescent modes must decay (see Crouch & Cally 2003, 2005, for details). The two-point boundary value problem is then solved numerically and the resultant complex wavenumber eigenvalues contain the information about the phase speed (real part of the eigenvalue) and mode conversion efficiency (imaginary part).

3. Genetic Magnetohelioseismology

To account for the observed radial variation of the magnetic field strength and inclination across a sunspot, we construct a simple model of concentric cylinders (or shells). Given the field strength, field inclination, and radial thickness of each shell, the eigenvalues can be used to calculate the resultant absorption and phase speed change produced by the model. We use a genetic algorithm to iteratively adjust the model parameters controlling the radial structure in order to find the best fit with observations. Figure 2 shows a typical result from this process. We have plotted the phase shifts (left hand side) and the absorption coefficients (right hand side) for the f mode and the first nine p modes. It is clearly evident that the observed phase shifts (diamonds with error bars) are remarkably well matched by our simple model (full curve). The absorption coefficients agree quite well. It is not readily apparent in Figure 2 but it has been shown by Cally et al. (2003) and Crouch et al. (2005) that these models can produce ample absorption to explain the observations.

4. Consequences for Sunspot Seismology

It is a commonly held perception that the observed phase speed increase is indicative of an enhanced sound speed in the subphotospheric layers of sunspots (see also Fan et al. 1995; Duvall et al. 1996; Kosovichev et al. 2000). Our results show that this is not the only explanation – those effects may be primarily magnetic in origin. The sound speed in our magnetic models is actually slightly reduced in comparison to the non-magnetic quiet Sun model (see Figure 1). Yet the resultant phase shifts produced by our simple sunspot models can agree remarkably well with the observations (depending on the specifics of the radial structure). Further work is needed to determine if this conclusion holds true in more complex models.

5. Testing the Upper Boundary Condition

In this section we present some preliminary results from a model that relaxes the rigid lid boundary condition (as employed by Crouch et al. 2005). Despite their

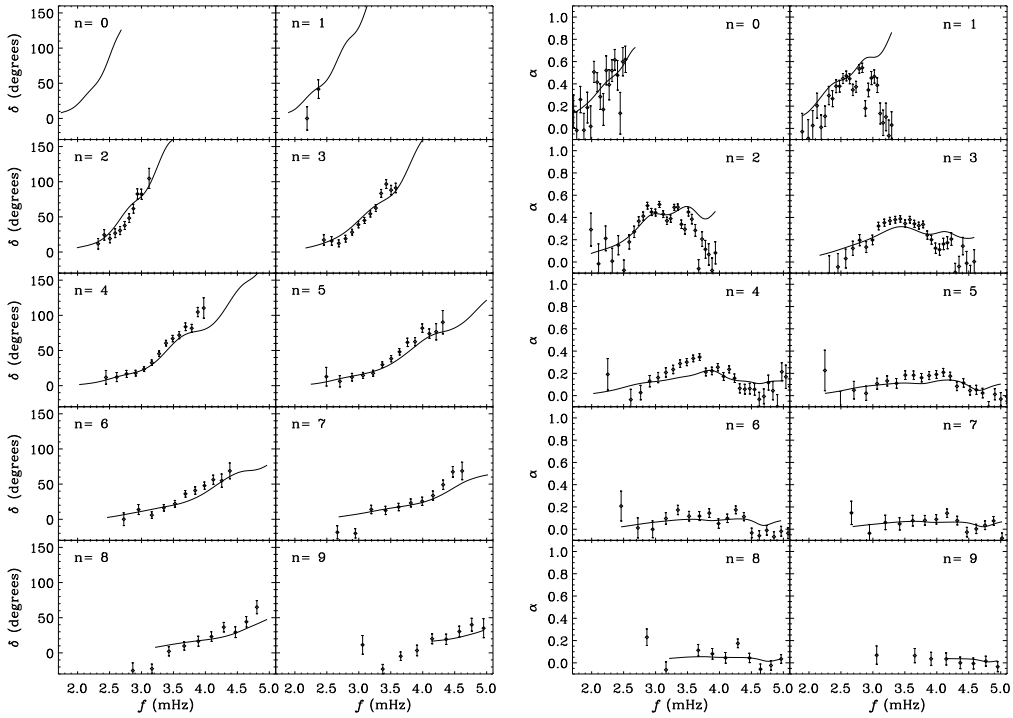

Figure 2. A comparison of the observations and theoretical predictions produced by a best fit five-shell model with: $B = \{3, 3, 3, 2, 2\}$ kG, $\theta = \{0, 45^\circ, 55^\circ, 55^\circ, 60^\circ\}$, and $R = \{1, 4.1, 5.78, 9.23, 12.53\}$ Mm. *Left:* Phase shift δ as a function of frequency for axisymmetric modes ($m = 0$) with radial orders $n = 0, \ldots, 9$. The *full curves* are the theoretical predictions and the *diamonds* (and associated error bars) are the observed m-averaged phase shifts for NOAA5254 (Braun 1995). Only observational data points which satisfy $\sigma_\delta < 18^\circ$ are displayed. *Right:* Same as the plot on the left, except the absorption coefficient α is plotted, and only observational data points which satisfy $\sigma_\alpha < 0.2$ are shown. From Crouch et al. (2005).

limitations in the atmosphere, as a first approximation we retain the assumptions of field uniformity and small amplitude waves. We model the atmosphere above the photosphere with two isothermal slabs. The gravitational acceleration is constant throughout the atmosphere and matches the value at the top of the solar interior model ($z = 500$ km). The lowest slab (which is intended to mimic the chromosphere) extends from $z = 500$ km to $z = 2000$ km, and has a temperature and adiabatic exponent that match the values at the top of underlying interior model. The upper slab is semi-infinite and has a temperature $T = 2 \times 10^6$ K (consistent with values observed in corona) and adiabatic exponent $\gamma = 5/3$.

It turns out that the linear wave equations for an isothermal slab permeated by a straight, uniform, inclined magnetic field can be solved analytically, when the direction of wave propagation is parallel to the vertical plane containing the magnetic field (*i.e.*, $\phi = 0$). In a similar fashion to the vertical field case (that was studied by Cally 2001), the solutions for inclined field problem can be written in terms of the hypergeometric ${}_2F_3$ functions (it should be pointed out

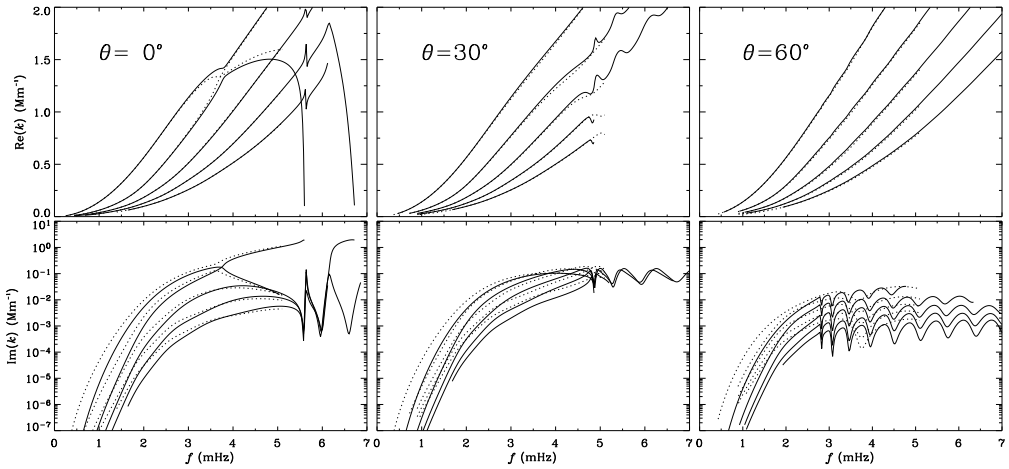

Figure 3. Complex wavenumber eigenvalues k as a function of frequency f for the modes with $n = 0, \ldots, 4$. The *top panels* show the real part of k as a function of f and the *bottom panels* show the corresponding imaginary part. The two *left hand panels* show results for exactly vertical field $\theta = 0$, the *middle panels* $\theta = 30°$, and the *right hand panels* $\theta = 60°$. In each case, the results from the model with an atmosphere placed above $z = 500$ km are plotted as full curves, and the results from the model with rigid lid boundary condition imposed at $z = 500$ km are plotted as dotted curves. In general the real parts of these two curves are in indistinguishable. At low frequencies both $\mathrm{Re}\,(k)$ and $\mathrm{Im}\,(k)$ are largest for $n = 0$ and decrease with increasing radial order n. For all these graphs the magnetic field strength is fixed at $B = 2$ kG and the propagation direction is fixed at $\phi = 0$ (so the Alfvén waves are decoupled in all these cases).

that Zhugzhda & Dzhalilov 1984, solved the same equations in terms of Meijer functions but these are significantly more complicated than the ${}_2F_3$ functions). We impose physically consistent boundary conditions at $z \to \infty$, such that wave-like disturbances travel upward and evanescent modes decrease with increasing height. The fast MAG waves are refracted at great height by the increasing sound speed and have leading behaviour $\exp(-kz)$. The slow MAG waves have leading behaviour $\exp\left\{-(z/2H)\left[1 + 2ikH\cos\phi\tan\theta - \sec\theta\sqrt{\cos^2\theta - (\omega/\omega_{ac})^2}\right]\right\}$, which shows that the acoustic cutoff frequency ω_{ac} is effectively reduced by a factor of $\cos\theta$ in regions with inclined magnetic field (in comparison to the quiet Sun value). Complete details of these solutions will be presented elsewhere (Crouch 2006).

Some illustrative results are presented in Figure 3. In that figure we have plotted the real and imaginary parts of the wavenumber eigenvalues for three field inclinations. Cally et al. (1994) used a similar approach to investigate the vertical field model. Their results compare well to the results shown in the left hand panels of Figure 3, although some of the details are sensitive to the slight differences in the models (such as which modes turn over and terminate at $\mathrm{Re}\,(k) = 0$).

One particularly important point demonstrated by Figure 3 is that the real parts of the wavenumber eigenvalues are fairly insensitive to the specifics of

the upper boundary condition (in most cases the curves of the two models are indistinguishable). The real parts of the wavenumbers control the phase shift produced by the simple shell models (see Figure 2). Consequently, our conclusion regarding the interpretation of the phase speed changes is unmodified (see Section 4. though the influence of field non-uniformity and non-linear wave dynamics in the atmosphere are yet to be tested).

On the other hand, the imaginary part of the wavenumbers (which control the absorption) are more sensitive to the nature of the upper boundary condition. At lower frequencies it appears that the magnitude of $\mathrm{Im}\,(k)$ is actually slightly reduced in the model that allows waves to propagate upward. At higher frequencies the difference between the two models is quite dramatic. The oscillations of $\mathrm{Im}\,(k)$, exhibited by the model with an atmosphere, are due to standing wave resonances in the cavity between the temperature minimum region ($z \approx 500$ km) and the transition region (the discontinuity separating the chromosphere and corona at $z = 2000$ km). It is evident that the resonances occur at lower frequencies in models with larger field inclination. This is to be expected because the acoustic cutoff frequency f_{ac} is inclination dependent (as explained above). For the $B = 2$ kG model in Figure 3, $f_{ac} = 5.46$ mHz in vertical field, $f_{ac} = 4.73$ mHz when $\theta = 30°$, and $f_{ac} = 2.73$ mHz when $\theta = 60°$. Those values are in very good visual agreement with the frequencies where the resonances commence. Waves below these frequencies will not form resonances as they do not propagate in the model chromosphere. Apart from the resonances, the average overall magnitude of the imaginary parts is quite similar to the rigid lid model (though the rigid lid values tend to provide an upper bound).

As we have discussed, this model is quite simplistic, but there are several questions that we intend to investigate: (1) how much acoustic energy is channelled from the p modes into the solar atmosphere; (2) what are the resultant absorption coefficients (especially at higher frequencies) and how do they compare with observations (*e.g.*, Braun 1995; Lindsey & Braun 1999); and (3) can useful information about the mode conversion process be extracted by comparing the displacements in the photospheric layers with observations? Some of these questions will be pursued in a forthcoming publication (Crouch 2006).

References

Bogdan, T. J., et al. 2003, ApJ, 599, 626
Braun, D. C. 1995, ApJ, 451, 859
Cally, P. S. 2001, ApJ, 548, 473
Cally, P. S., Bogdan, T. J., & Zweibel, E. G. 1994, ApJ, 437, 505
Cally, P. S., Crouch, A. D., & Braun, D. C. 2003, MNRAS, 346, 381
Christensen-Dalsgaard J. 1997, Aarhus adiabatic pulsation package, `http://www.obs.aau.dk/~jcd/adipack.n/`
Crouch, A. D., & Cally, P. S. 2003, Solar Phys., 214, 201
Crouch, A. D., & Cally, P. S. 2005, Solar Phys., 227, 1
Crouch, A. D., Cally, P. S., Charbonneau, P., Braun, D. C., & Desjardins, M. 2005, MNRAS, 363, 1188
Crouch, A. D. 2006, MNRAS, in preparation
Duvall, T. L., Jr., D'Silva, S., Jefferies, S. M., Harvey, J. W., & Schou, J. 1996, Nat, 379, 235
Fan, Y., Braun, D. C., & Chou, D.-Y. 1995, ApJ, 451, 877

Kosovichev, A. G., Duvall, T. L., Jr., & Scherrer, P. H. 2000, Solar Phys., 192, 159
Lindsey, C., & Braun, D. C. 1999, ApJ, 510, 494
Rosenthal, C. S., et al. 2002, ApJ, 564, 508
Zhugzhda, I. D. & Dzhalilov, N. S. 1984, A&A, 132, 45